Chapter 15
Noncovalent Interactions of Organic Ions with Polar Molecules in the Gas Phase

M. Samy El-Shall, Isaac K. Attah and Sean P. Platt

Abstract The chapter is focused on noncovalent interactions of organic ions with small polar molecules in the gas phase. The organic ions studied include cyclic $C_3H_3^+$ and the radical cations of benzene ($C_6H_6^{\bullet+}$), pyridine ($C_5NH_5^{\bullet+}$), pyrimidine ($C_5N_2H_4^{\bullet+}$), fluorobenzene ($C_6H_5F^{\bullet+}$), phenylacetylene ($C_8H_6^{\bullet+}$), benzonitrile ($C_7NH_5^{\bullet+}$) and naphthalene ($C_{10}H_8^{\bullet+}$). In addition, protonated pyridine (pyridine.H$^+$) and protonated pyrimidine (pyrimidine.H$^+$) are also included for comparison with the radical cations. The solvent molecules include water (H_2O), hydrogen cyanide (HCN) and acetonitrile (CH_3CN). The results presented include experimental thermochemical data (ΔH° and ΔS°) for the stepwise association of the solvent molecules with the organic ions and theoretically calculated binding energies and structures. The four major topics discussed are: (1) Trends in binding energies and entropy changes, (2) Ionic hydrogen bonds with organic ions, (3) Internal vs. external solvation of the organic ions, and (4) Intracluster proton transfer and deprotonation of the organic ions.

15.1 Introduction

Intermolecular forces, including hydrogen bonds and ion-molecule interactions, [1–5] are important in many biological, chemical, and astrochemical processes such as the conformation and folding of proteins, base pair stacking in DNA, drug design, macromolecular assemblies, molecular recognition, clathrate hydrate formation, and the formation of complex organics and ices in interstellar space [1–7].

A special class of hydrogen bonding interactions, usually referred to as ionic hydrogen bonds (IHBs), involves hydrogen bonding between radical ions or protonated molecules and neutral polar molecules such as water, methanol, ammonia, and hydrogen cyanide [1]. IHBs have bond strengths higher than the typical

M. S. El-Shall (✉) · I. K. Attah · S. P. Platt
Department of Chemistry, Virginia Commonwealth University, 23284–2006 Richmond, VA, USA
e-mail: mselshal@vcu.edu

M. S. El-Shall
Department of Chemistry, Faculty of Science, King Abdulaziz University,
Jeddah 21589, Saudi Arabia

conventional hydrogen bond in neutral systems and could reach up to 35 kcal/mol, nearly a third of the strength of covalent bonds [1]. These strong interactions are critical in many fields such as ion induced nucleation, ionic clusters, ion solvation, radiation chemistry, electrochemistry, acid-base chemistry, and self-assembly in supramolecular chemistry [1–5]. IHBs are also important in biological systems including protein folding, proton transport, membranes, enzyme active centers, and molecular recognition [8, 9] Organic ions can form hydrogen bonds with solvents in nature, for example, in icy grains doped with polycyclic aromatic hydrocarbons that are subjected to ionizing radiation in interstellar dust grains [10–13].

Unconventional carbon-based IHBs are formed when the hydrogen donors are ionized hydrocarbons containing CH groups and the hydrogen acceptors are electron lone pairs on hetero atoms such as O and N or π electrons in olefin double bonds and aromatic systems [1]. For example, carbon-based $CH^{\delta+}$–O IHBs appear in the hydration of ionized aromatics such as benzene ($C_6H_6^{\bullet+}$), cyclic $C_3H_3^+$, cyclobutadiene ($C_4H_4^{\bullet+}$), phenylacetylene ($C_8H_6^{\bullet+}$), and naphthalene ($C_{10}H_8^{\bullet+}$) [14–19]. Organic ions can also interact with water molecules by stronger conventional hydrogen bonds, such as in protonated pyridine or protonated pyrimidine where the NH^+–O hydrogen bonds are formed [1, 20, 21].

In addition to water, other polar molecules containing lone pairs of electrons such as hydrogen cyanide, methanol, and acetonitrile can participate in hydrogen bonding interactions with the ring hydrogen atoms ($CH^{\delta+}$) of ionized aromatics. Hydrogen cyanide is a useful probe of non-covalent interactions because it is highly polar (dipole moment = 2.98 D), [22] and it can serve both as a hydrogen donor and as a lone-pair hydrogen acceptor in hydrogen bonds [1]. HCN has received considerable attention because of its role in atmospheric chemistry as a result of its release by biomass burning, [23] and it is also one of the main interstellar/nebula molecules [13]. HCN can be produced in space from the reactions of ammonia and methane, and could play a very important role in the formation of nitrogen-containing polycyclic aromatic hydrocarbons (NPAHs) [24]. Since molecules in outer space are subjected to ionizing radiation from stars, radioactive decay and cosmic rays, ionized aromatics such as benzene and PAHs may act as nucleation centers for the condensation of astrochemical molecules such as hydrogen cyanide to form clusters that could undergo intracluster reactions leading to nitrogen containing PAHs [6, 24]. Nitrogen-containing aromatics are of interest because biologically significant molecules such as DNA, RNA, and certain amino acids and proteins contain nitrogen-substituted rings. As a result, a fundamental understanding of the reactions and structures of nitrogen-containing species in space may provide insights into the origin of life [24–26]. In fact, HCN polymers have been shown to exist in meteorites, comets, planets, moons, and in circumstellar envelopes [24, 27, 28].

Insight into the basic molecular interactions can be obtained from the energies and structures of the key species involved in the stepwise association of polar molecules with organic ions. These data can be obtained experimentally by measuring sequential binding energies of solvent molecules to organic ions in the gas phase, and computationally by calculating the structures and binding energies of the hydrated and solvated organic ions [1,14–21, 29–32]. One of the most established methods for

measuring binding energies of solvent molecules to organic ions in the gas phase is the mass-selected ion mobility (MSIM) method which allows measurements of thermochemical equilibria between a mass-selected ion and several solvent molecules (typically 1–6) [14–21, 30–32]. These measurements, when conducted at different temperatures, yield enthalpy and entropy changes associated with the stepwise association of solvent molecules with the organic ions. A good deal of work over the last decade or two has been conducted using equilibrium measurements to obtain thermochemical data on the stepwise solvation of organic ions with a variety of solvent molecules including water [1, 33–42]. This work continues to this day, with a focus on trends in binding energies and correlations with the properties of the solvent molecule such as dipole moment and proton affinity, and the nature of the organic ion including size, charge distribution and degree of charge delocalization. Our group has been active in studying the stepwise hydration and solvation of different types of organic ions, and this chapter provides an overall review of these recent studies [14–21, 43–48]. In particular, we focus on the interactions of organic ions with three solvent molecules: water, hydrogen cyanide and acetonitrile. We specifically address three issues: (1) variation of binding energies with the structures and properties of the solvent molecules, (2) the onset of ion solvation involving a small number (four to six) of solvent molecules and whether internal or external solvation is preferred, and (3) the degree of intracluster proton transfer within the solvated ions and the ability of a number of solvent molecules to abstract a proton from the organic ion to form a more stable protonated solvent cluster and covert the organic radical cation into a radical which could be more reactive in addition reactions with small organic molecules.

The review begins with a brief description of the MSIM technique to carry out the thermochemical equilibrium measurements to determine the sequential binding energies and entropy changes of the stepwise solvation of organic ions. The next section describes the main experimental and computational results for the solvation of organic ions. Attention is focused on: (1) Trends in Binding Energies & Entropy Changes, (2) Structures of the Hydrated/Solvated Ions, (3) Internal vs. External Solvation, and (4) Intracluster Proton Transfer & Deprotonation Reactions.

15.2   Experimental Measurements of Sequential Enthalpy and Entropy Changes

Figure 15.1 illustrates the essential components of the ion mobility system at Virginia Commonwealth University (VCU) [17, 18, 21]. In the experiments, mass-selected ions (generated by electron impact ionization of the neutral molecules or clusters) are injected (in 20–30 μs pulses) into the drift cell containing a helium carrier gas typically at 1 Torr containing a known partial pressure of the solvent vapor. Flow controllers are used to maintain a constant pressure inside the drift cell. The drift cell temperature can be set within the range of 78–773 K, and can be controlled to ± 1 K using four temperature controllers, using liquid nitrogen flowing through actuated solenoid valves to cool down the drift cell for temperature experiments below room
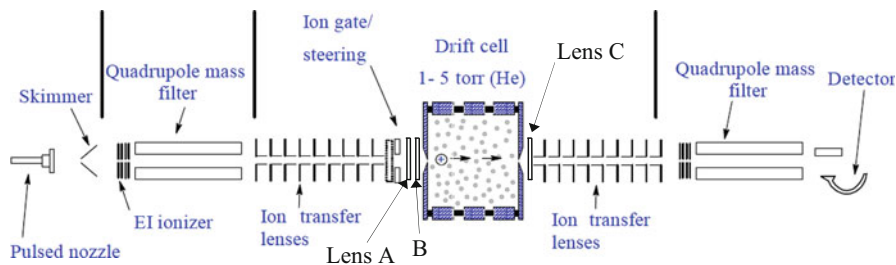
Fig. 15.1 VCU mass-selected ion mobility system [18]

temperature. The reaction products can be identified by scanning a second quadrupole mass filter located coaxially after the drift cell. The arrival time distributions (ATDs) are collected by monitoring the intensity of each ion as a function of time. The reaction time can be varied by varying the drift voltage. Most of the ion thermalization occurs outside the cell entrance by collisions with the solvent vapor escaping from the cell entrance orifice. At a cell pressure of 0.2 Torr, the number of collisions that the ion encounters with the solvent molecules within the 1.5 ms residence time inside the cell is about 10^4 collisions, which is sufficient to ensure efficient thermalization of most of the organic ions.

Figures 15.2a and 15.2b show typical examples of mass spectra obtained following the injection of the mass-selected pyrimidine and benzene radical cations into the drift cell containing water and HCN vapors, respectively [21, 45]. In the absence of water in the drift cell (Fig. 15.2a), only the mass-selected pyrimidine radical cation is observed as shown in Fig. 15.2a (top). In the presence of water, both the $(C_4N_2H_4^{\bullet+})(H_2O)_n$ with $n = 1$–5 and the protonated water series $H^+(H_2O)_n$ with $n = 4$–9 are observed [21]. They consistently shift towards higher n as the temperature of the drift cell decreases. For example, at 238 K the observed ions are $(C_4N_2H_4^{\bullet+})(H_2O)_n$ with $n = 2$–5 and $H^+(H_2O)_n$ with $n = 5$–9 as shown in Fig. 15.2a (bottom). The formation of protonated water clusters $H^+(H_2O)_n$ with $n \geq 4$ is attributed to the dissociative proton transfer reactions represented by Reaction 1 below Eq. (15.1):

$$[C_4H_4N_2^{\bullet+}(H_2O)_{n-1}] + H_2O \rightarrow C_4H_3N_2^{\bullet} + [H^+(H_2O)_n]; n \geq 4 \qquad (15.1)$$
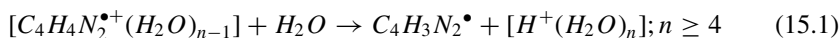
Similar dissociative proton transfer reactions have been observed in the hydration of benzene and the cyclic C_3H_3 cations [14–16]. These reactions are further discussed in Sect. 15.2.4.

In Fig. 15.2b, the injection of the mass-selected $C_6H_6^{\bullet+}$ ion into the drift cell containing 0.1 Torr HCN vapor at 298 K, results in the formation of the association products $C_6H_6^{\bullet+}(HCN)_n$ with $n = 1$ and 2 [45]. At 178 K (the lowest achievable temperature before the condensation of HCN), the cluster population is dominated by the $C_6H_6^{\bullet+}(HCN)_n$ series from $n = 2$ to 6 with $n = 3$ and 4 being the major ions observed as shown in Fig. 15.2b (bottom) [45].
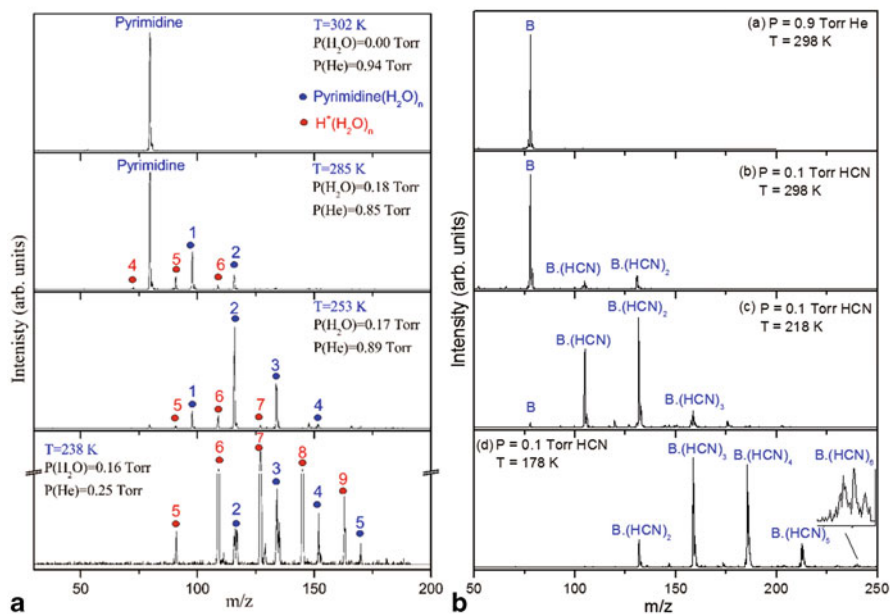
Fig. 15.2 a Mass spectra resulting from the injection of the mass-selected pyrimidine radical cation $(C_4N_2H_4^{\bullet+})$ into a helium (He)—water (W) vapor mixture at different temperatures using 12.7 eV injection energy (*laboratory frame*) and 2.5 V/cm drift field [21]. **b** Mass spectra obtained following the injection of the mass-selected $C_6H_6^{\bullet+}$ (B) into the drift cell containing He and HCN vapor at different pressures and temperatures as indicated [45]

A good test of equilibrium is the observation of identical ATDs of the reactant and product ions. If the $I^{\bullet+}(S)_{n-1}$ and $I^{\bullet+}(S)_n$ ions are in equilibrium, their ATDs must be identical [15–17, 22]. This is evident from the ATDs of the $(C_4N_2H_4^{\bullet+})(H_2O)_n$ ions with $n = 1–5$ as shown in Fig. 15.3a. The ion intensity ratio $I^{\bullet+}(S)_n/I^{\bullet+}(S)_{n-1}$ is measured from the integrated peak areas of the ATDs as a function of decreasing cell drift field corresponding to increasing reaction times, and equilibrium is achieved when a constant ratio is obtained. The equilibrium constants are then obtained using Eq. (15.2).

$$K_{eq} = [I^{\bullet+}(S)_n]/[I^{\bullet+}(S)_{n-1}]P(S) \tag{15.2}$$

Here, $[I^{\bullet+}(S)_n]$ and $[I^{\bullet+}(S)_{n-1}]$ are the intensities of the peaks taken from the integrated ATDs, and P(S) is the partial pressure of the solvent (S) in atm. The equilibrium constants measured as a function of temperature yield $\Delta H°$ and $\Delta S°$ from the slopes and intercepts, respectively of the van't Hoff plots as illustrated by the typical examples shown in Fig. 15.3b.
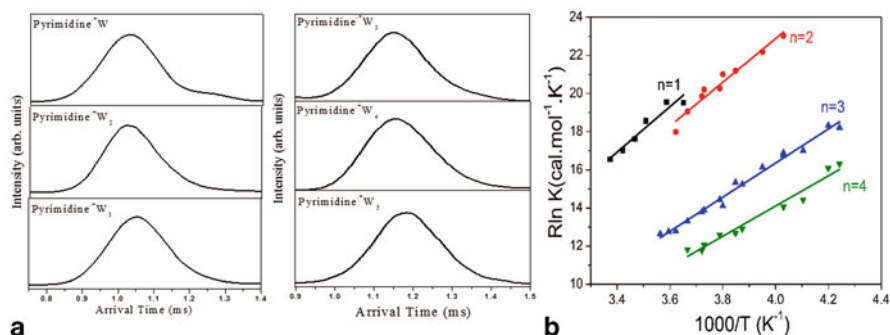
Fig. 15.3 a (*Left*) ATDs of the pyrimidine$^{\bullet+}$(H$_2$O)$_n$ ions with $n = 1$–3 collected following the injection of mass-selected pyrimidine$^{\bullet+}$ into the drift cell containing 0.21 Torr water vapor + 0.22 Torr helium buffer gas at 268 K. (*Right*) ATDs of the pyrimidine$^{\bullet+}$(H$_2$O)$_n$ ions with $n = 3$–5 collected following the injection of mass-selected pyrimidine$^+$ into the drift cell containing 0.19 Torr water vapor and 0.22 Torr of helium buffer gas at 243 K [21]. **b** van't Hoff plots of the temperature dependence of the equilibrium constant of the stepwise hydration of the pyrimidine radical cation and formation of pyrimidine$^{\bullet+}$(H$_2$O)$_n$ with $n = 1$–4 [21]

Table 15.1 Ionization energies and proton affinities of the studied aromatic and polar molecules [22]. The dipole moments (μ) of the polar molecules are also included

Compound	Ionization energy (eV)	Proton affinity (kcal/mol)
Benzene	9.2	179.3
Phenylacetylene	8.8	198.9
Fluorobenzene	9.2	180.7
1,4 di-Fluorobenzene	9.2	171.8
Benzonitrile	9.7	194.0
Naphthalene	8.1	191.9
Pyridine	9.3	222.0
Pyrimidine	9.3	211.7
H$_2$O ($\mu = 1.9$ D)	12.6	165.0
CH$_3$OH ($\mu = 1.7$ D)	10.8	180.3
HCN ($\mu = 2.98$ D)	13.6	179.4
CH$_3$CN ($\mu = 3.9$ D)	12.2	186.2

15.2.1   Trends in Binding Energies & Entropy Changes

Table 15.1 lists molecular properties relevant to the organic ions and solvent molecules discussed in this chapter [22]. Tables 15.2, 15.3, 15.4 list the enthalpy and entropy changes corresponding to the association of water, hydrogen cyanide, and acetonitrile, respectively with different organic ions.

Table 15.2 Thermochemistry of hydrated organic cations

Cation (Ref)	$-\Delta H^o$(kcal/mol)	$-\Delta S^o$(cal mol^{-1} K^{-1})	ΔE (Calc) (kcal/mol)
Cyclic $C_3H_3^+$ [16]	11.7	18.8	11.8
Benzene$^{•+}$ [15]	9.0	19.5	8.5
Phenylacetylene$^{•+}$ [17]	8.0	17.8	7.8
Benzonitrile$^{•+a}$	11.5	29.4	7.7
Naphthalene$^{•+}$ [19]	7.8	19.5	7.7
Pyridine$^{•+}$ [20]	15.2	33.1	15.4 (distonic ion) 10.2 (conventional)
Protonated pyridine [20]	15.6	27.0	14.5
Pyrimidine$^{•+}$ [21]	11.9	23.6	10.8
Protonated pyrimidine [21]	16.7	38.6	16.9

[a] Unpublished results

Table 15.3 Thermochemistry of HCN complexes with organic cations

Cation (Ref)	$-\Delta H^o$ (kcal/mol)	$-\Delta S^o$ (cal mol^{-1} K^{-1})	ΔE (Calc) (kcal/mol)
Benzene$^{•+}$ [45]	9.2	19.1	9.4
Phenylacetylene$^{•+}$ [46]	10.5	24.6	9.5
F-benzene$^{•+}$ [47]	11.2	24.4	9.6
1,4-di F-benzene$^{•+}$ [47]	11.2	22.5	9.8
Benzonitrile$^{•+}$ [47]	9.6	19.1	9.5
Naphthalene$^{•+a}$	6.8	15.3	7.8
Pyridine$^{•+}$ [48]	11.4	21.8	11.9
Protonated pyridine [48]	14.0	26.6	16.0
Pyrimidine$^{•+}$ [48]	12.0	23.3	12.7

[a] Unpublished results

Figure 15.4a compares the hydration energies and the sequential binding energies of several water molecules to the c-$C_3H_3^+$, benzene ($C_6H_6^{•+}$), phenylacetylene ($C_6H_5CCH^{•+}$) and naphthalene ($C_{10}H_8^{•+}$) ions. The hydration energy is the largest for the c-$C_3H_3^+$ (11.7 kcal/mol) followed by the benzene and the phenylacetylene cations (9.0 and 8.0 kcal/mol, respectively), and then the naphthalene cation (7.8 kcal/mol). The range of the hydration energies is consistent with the usual strength of ionic hydrogen bonds of the type $CH^{\delta+} \cdots OH_2$ which are typically about 9 kcal/mol [1]. The IHB in the hydrated c-$C_3H_3^+$ is nearly 50 % stronger than in the respective hydration of the naphthalene cation due to the higher charge density on the $C_3H_3^+$

Table 15.4 Thermochemistry of CH_3CN complexes with organic cations

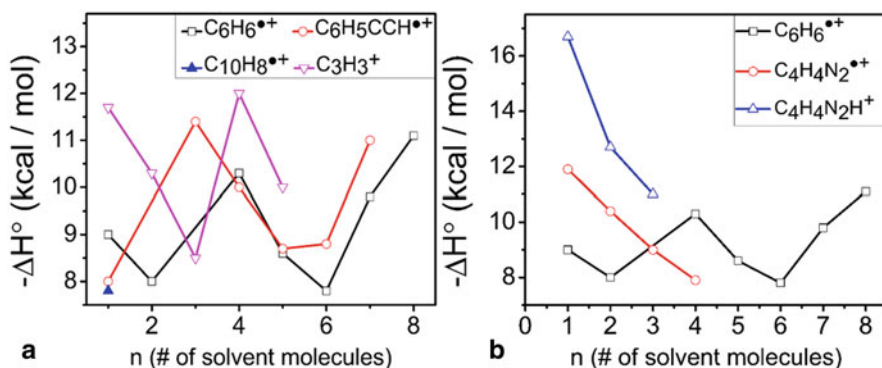| Cation (Ref)	$-\Delta H^o$ (kcal/mol)	$-\Delta S^o$ (cal mol^{-1} K^{-1})	ΔE (Calc) (kcal/mol)
$C_3H_3^+$ [16]	15.3	21.5	–
Benzene$^{•+}$ [45]	14.0	19.9	13.0
Protonated Pyrimidine [21]	–	–	23.7
Naphthalene$^{•+a}$	11.2	20.3	10.8

[a] Unpublished results

Fig. 15.4 a Sequential binding energies of water molecules to the c-$C_3H_3^+$, benzene ($C_6H_6^{•+}$), phenylacetylene ($C_6H_5CCH^{•+}$) and naphthalene ($C_{10}H_8^{•+}$) cations [15–17, 19]. **b** Sequential binding energies of water molecules to the benzene ($C_6H_6^{•+}$) and pyrimidine ($C_4H_4N_2^{•+}$) radical cations and to protonated pyrimidine ($C_4H_4N_2H^+$) [15, 21]

ion as compared to the $C_{10}H_8^{•+}$ ion. The charge delocalization over the bicyclic naphthalene cation decreases the charge-dipole interaction of the $CH^{\delta+}\cdots OH_2$ bond in the naphthalene$^{•+}$(H_2O) complex.

For both the c-$C_3H_3^+$ and the benzene cation, an increase in the binding energy of the fourth water molecule is observed and for the phenylacetylene cation this increase is observed for the addition of the third water molecule. This could suggest the formation of geometrically stable structures of the first solvent shell around the ion as shown from the DFT calculations discussed in Sect. 15.2.3.

Another interesting result is the apparent increase in the sequential binding energies associated with the formation of the benzene$^{•+}$(H_2O)$_7$, benzene$^{•+}$(H_2O)$_8$, and phenylacetylene$^{•+}$(H_2O)$_7$ clusters. The formation of these large clusters is also associated with large entropy changes (-25.5, -32.6 and -32 cal/mol K, respectively) as compared to the nearly constant $-\Delta S^o$ value of 20 ± 3 cal/mol K for the $n = 1$–5 clusters [15, 17]. This could suggest strong orientational restraint of water in the larger clusters [49]. In fact, three-dimensional cage-like structures involving multiple rings sharing edges are the lowest energy conformers of the water heptamer and octamer [49, 50]. The observed large negative entropy of the phenylacetylene$^{•+}$(H_2O)$_7$ and

benzene$^{\bullet+}$(H$_2$O)$_8$ clusters could be explained by the formation of cage-like structures by 7–8 H$_2$O molecules similar to neutral water clusters [49, 50]. This observation could be related to the common bulk view of hydrophobic hydration where water molecules tend to organize around small hydrophobic units without sacrificing hydrogen bonds [51]. The entropy loss associated with this organization is the major reason for the low solubility of nonpolar organic molecules in water [51]. However, in the hydration of large organic ions such as benzene and phenylacetylene, it is not theoretically confirmed that the organization of water molecules into cage-like structures would incorporate such organic ions within the cages.

Figure 15.4b compares the sequential hydration energies of the pyrimidine radical cation (C$_4$H$_4$N$_2^{\bullet+}$) and protonated pyrimidine (C$_4$H$_4$N$_2$H$^+$) with those of the benzene radical cation. With the protonated pyrimidine, water is bonded by a conventional NH$^+$$\cdots$OH$_2$ bond which is significantly stronger (16.7 kcal/mol) than the unconventional CH$^{\delta+}$$\cdots$OH$_2$ bond (8–9 kcal/mol) [21]. Also, the hydration energy of the pyrimidine cation (11.9 kcal/mol) is higher than that of the benzene cation (9.0 kcal/mol) although in both cases the water binds to a CH$^{\delta+}$ site by an unconventional IHB (CH$^{\delta+}$$\cdots$OH$_2$) as indicated by the DFT calculations of the lowest energy structures [15, 21]. The sequential binding energies of the pyrimidineH$^+$(H$_2$O)$_n$ clusters decrease with n and approach the limiting macroscopic value of 10.5 kcal/mol, the condensation energy of water at $n = 3$ [21]. This follows the usual trend in systems with conventional ionic hydrogen bonds [1]. However, this trend is clearly different from the hydration of the benzene cation as shown in Fig. 15.4b. In relation to these data, the C-H hydrogens of the pyrimidine radical cation (C$_5$H$_4$N$_2^{\bullet+}$) can only form carbon-based CH$^{\delta+}$$\cdots$OH$_2$ bonds to water, similar to those formed by the benzene$^{\bullet+}$ ion [14, 15]. In fact, DFT calculations below also show that the hydrogen bond strength of the pyrimidine$^{\bullet+}$ ion to water is 10.8 kcal/mol, in good agreement with the measured value of 11.9 kcal/mol [21].

The hydration energy of protonated pyrimidine measured by the MSIM method (16.7 kcal/mol) is consistent with the hydration energies of other aromatic ions recently measured using energy-resolved collision-induced dissociation (CID) [29]. For example; the CID hydration energies of protonated aniline, acetophenone and phenol were measured as 14.4, 15.6 and 17.5 kcal/mol, respectively [29]. The hydration energy of protonated pyrimidine is higher than that of aniline and slightly lower than of that phenol. The measured hydration energies appear to correlate well with the proton affinity of the aromatic molecules as shown in Tables 15.1 and 15.2 [1].

Figure 15.5a compares the sequential binding energies of HCN molecules with protonated pyridine and the radical cations of pyrimidine, pyridine, phenylacetylene, and benzene. The binding of multiple HCN molecules to the benzene cation is mostly due to unconventional CH$^{\delta+}$–NCH hydrogen bonds directly connected to the CH$^{\delta+}$ sites of the benzene cation and also hydrogen bonding chains (HCN–HCN) among the HCN molecules [45]. The small difference in the bond strength of the two types of interactions (CH$^{\delta+}$–NCH and HCN–HCN) results in relatively small changes of $(-\Delta H_{n-1,n}^{\circ})$ for $n = 1$–4 as shown in Fig. 15.5a. HCN binds more strongly to the pyridine and pyrimidine radical cations due to ion-dipole interactions in addition to the CH$^{\delta+}$–NCH hydrogen bonding interactions [48]. The strongest binding of HCN
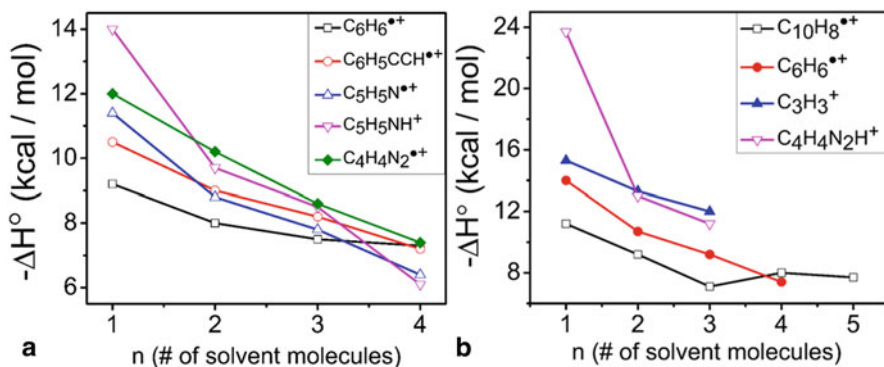
Fig. 15.5 **a** Sequential binding energies of HCN molecules to the benzene ($C_6H_6^{\bullet+}$), phenylacetylene ($C_6H_5CCH^{\bullet+}$), pyridine ($C_5H_5N^{\bullet+}$), and pyrimidine ($C_4H_4N_2^{\bullet+}$) radical cations, and protonated pyridine ($C_5H_5NH^+$) [45–48]. **b** Sequential binding energies of CH_3CN molecules to c-$C_3H_3^+$, benzene ($C_6H_6^{\bullet+}$), naphthalene ($C_{10}H_8^{\bullet+}$) and protonated pyrimidine ($C_4H_4N_2H^+$) [16, 45, 48]

is observed with protonated pyridine as shown in Fig. 15.5a. This bonding interaction is mainly due to an IHB that forms between the NH^+ group of the protonated pyridine and the N atom of HCN (NH^+–NCH bond). A significant drop in the binding energy (31 %) is observed upon the addition of the second HCN molecule to the protonated pyridine in contrast to the smaller changes observed upon the addition of the second HCN molecule to the pyridine or pyrimidine radical cations (23, and 15 %, respectively) as shown in Fig. 15.5a [48]. Despite the strong bonding of HCN to protonated pyridine, the interaction decreases sharply by further addition of HCN molecules and the binding of the fourth HCN molecule is only 6.1 kcal/mol [48]. In fact, in all of the studied HCN clusters around ionized or protonated aromatics, [45–48] the binding energies converge with the addition of 4–5 HCN molecules to the enthalpy of vaporization of HCN liquid (ΔH^o_{vap}), which is 6.0 kcal/mol at 298 K [22].

Figure 15.5b compares the sequential binding energies of acetonitrile molecules to protonated pyrimidine, c-C_3H_3 cation and benzene and naphthalene radical cations. DFT calculations indicate that acetonitrile forms a strong proton-bound dimer with protonated pyrimidine (calculated binding energy = 23.7 kcal/mol) [46]. This is a consequence of the large dipole moment of acetonitrile (3.9 D) as compared to 1.6 D for water. As a result, the ion-dipole interaction term is stronger in the case of acetonitrile, and the overall binding energy is significantly higher in pyrimidineH$^+$(NCCH$_3$) (23.7 kcal/mol) than in pyrimidineH$^+$(OH$_2$) (16.7 kcal/mol) [21, 48].

Figure 15.5b also shows a significant drop in the binding energy (43 %) upon the addition of the second acetonitrile molecule to the proton-bound dimer $(C_4N_2H_4)H^+$(NCCH$_3$) as compared to the water interactions where the corresponding drop in binding energy is 24 % as shown in Fig. 15.4b. The transition from strong ionic hydrogen bonding in the proton-bound dimer to weaker $CH^{\delta+}$–N type of bonds is responsible for the sharp drop in the binding energy of the $(C_4N_2H_4)H^+(CH_3CN)_2$ cluster. However, in the case of water, extended hydrogen bonding networks can be

formed as shown in the calculated low energy structures of the $(C_4N_2H_4)H^+(H_2O)_2$ clusters discussed in Sect. 15.2.3.

The effect of charge localization on the organic ion is clearly observed by comparing the binding energies of c-$C_3H_3^+(CH_3CN)_n$ and naphthalene$^{\bullet+}(CH_3CN)_n$ clusters shown in Fig. 15.5b. The naphthalene$^{\bullet+}(CH_3CN)_n$ clusters show the weakest sequential binding energies among the ions shown in Fig. 15.5b. This is again a result of charge delocalization on the naphthalene radical cation which leads to weaker charge-dipole interactions in comparison with the c-$C_3H_3^+(CH_3CN)_n$ clusters.

15.2.2 $CH^{\delta+}\ldots O$ and $CH^{\delta+}\ldots N$ Ionic Hydrogen Bonds with Organic Ions

The calculated lowest energy structures of several hydrated ions along with their calculated binding energies (kcal/mol) are shown in Fig. 15.6. Except for the protonated pyrimidine, protonated pyridine and distonic pyridine ion, all the ions show unconventional IHBs of the type $CH^{\delta+}\cdots OH_2$. For the c-$C_3H_3^+(H_2O)$, a single hydrogen bond between the water oxygen atom and one of the $C_3H_3^+$ hydrogen atoms is formed. The charges on c-$C_3H_3^+$ are equally distributed and localized among the carbon atoms (90 % of the charge) [16]. Upon clustering with one water molecule, the charge distribution changes with significant localizations on the hydrogen atoms of the c-$C_3H_3^+$, and one C-H bond shows elongation resulting from the linear H-bond formation with the oxygen atom of the water molecule [16].

For the benzene$^{\bullet+}$, phenylacetylene$^{\bullet+}$, naphthalene$^{\bullet+}$, and pyrimidine$^{\bullet+}$ radical cations, the lowest energy hydrated ion has a bifurcated structure with H_2O bonding to two CH hydrogens as shown in Fig. 15.6. This structure was also found in several *ab initio* studies of the benzene$^{\cdot+}(H_2O)$ cluster [52–57]. The MP2 corrected binding energy of 8.5 kcal/mol (Table 15.1) matches well the experimental value of 9.0 ± 1 kcal/mol, [15] and that reported from the IR photodissociation experiment of 9.4 ± 0.3 kcal/mol of the benzene$^{\bullet+}(H_2O)$ cluster [58].

For the hydrated phenylacetylene cation, $C_8H_6^{\bullet+}(H_2O)$, another structure where the water molecule is attached to the hydrogen of the acetylene group is only 1 kcal/mol higher in energy than the lowest energy isomer (at the MP2//ROHF/6-31+G** level) [17]. This indicates that the hydration of the organic ions could involve several structures with energetically similar binding sites. Experimentally, the observed equilibrium could involve different structural isomers depending on the relative stability of these isomers and the temperature of the experiment. As a result, the measured binding energy may represent an average value for water binding to different hydrogen atoms on the ion.

For the hydrated naphthalene cation, the two lowest energy isomers (at the B3LYP/6-311++G** level) have bifurcated structures with H_2O bonding to two CH hydrogens as shown in Fig. 15.6d [19]. The bifurcated structures have significantly larger binding energies than the ion-dipole structure where the water molecule lies above the plane of the naphthalene cation [19]. Also the calculated binding energies
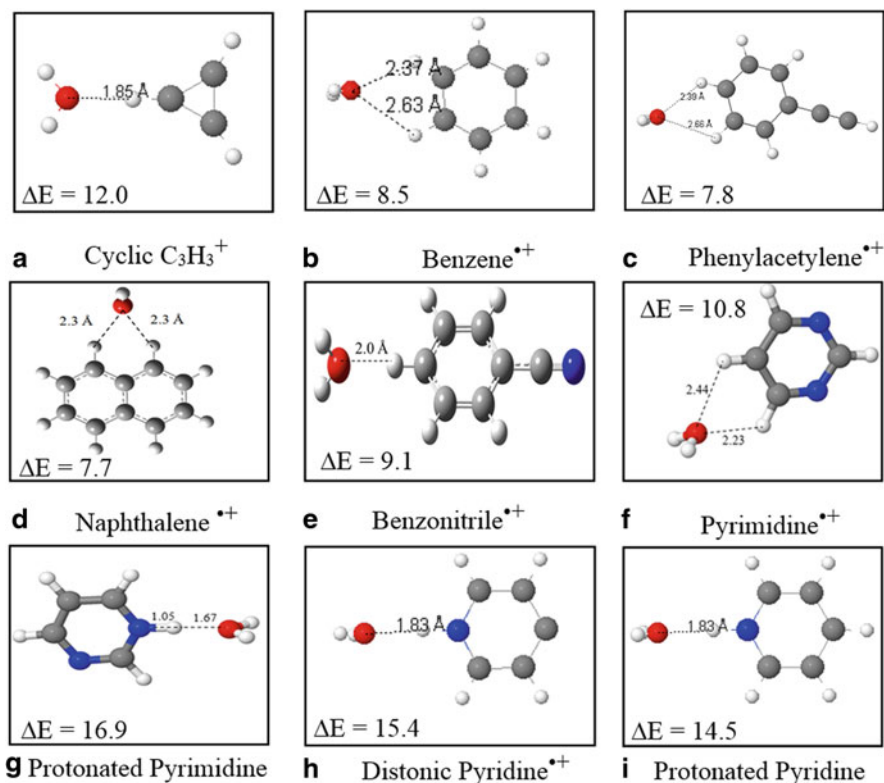
Fig. 15.6 Lowest energy structures of hydrated organic cations. ΔE is the calculated binding energy in kcal/mol. The calculated structures were obtained at the MP2//ROHF/6-31+G(d, p) level for the c-$C_3H_3^+$, benzene$^{\bullet+}$, phenylacetylene$^{\bullet+}$, pyridine$^{\bullet+}$, distonic pyridine$^{\bullet+}$ and protonated pyridine cations, [15–17,20] at the B3LYP/6-311++G(d, p) level for the naphthalene$^{\bullet+}$ and benzonitrile$^{\bullet+}$, [19] and at the M06-2X/6-311++G(d, p) level for the pyrimidine$^{\bullet+}$ and protonated pyrimidine [21]

of the bifurcated structures (7.7–6.8 kcal/mol) are in good agreement with the experimentally determined value (7.8 ± 1 kcal/mol) [19].

For the hydration of the pyridine radical cation, the measured binding energy of the pyridine$^{\bullet+}$(H_2O) cluster (15.2 kcal/mol) was similar to that of the protonated pyridine-water cluster ($C_5H_5NH^+$)(H_2O) (15.6 kcal/mol) that involves a $NH^+\cdot\cdot OH_2$ bond, and different from those of the hydrated benzene radical cation (9.0 kcal/mol) (Table 15.2) [20]. These relationships indicated that the hydrated pyridine$^{\bullet+}$ ions have the distonic $^{\bullet}C_5H_4NH^+$ structure that can form $NH^+\cdot\cdot OH_2$ bonds [20]. The calculated $CH^{\delta+}\cdot\cdot OH_2$ binding energy for the conventional pyridine ion to one water molecule is 10.2 kcal/mol, which does not agree with the experimental measured value of 15.2 kcal/mol, while the calculated $NH^+\cdot\cdot OH_2$ binding energy of the distonic pyridine ion to one water molecule is 15.4 kcal/mol, in excellent agreement with the experimental measured values of 15.2 and 15.6 kcal/mol for the ($C_5H_5N^{\bullet+}$)(H_2O) and ($C_5H_5NH^+$)(H_2O) clusters, respectively [20]. However, the hydrated pyrimidine
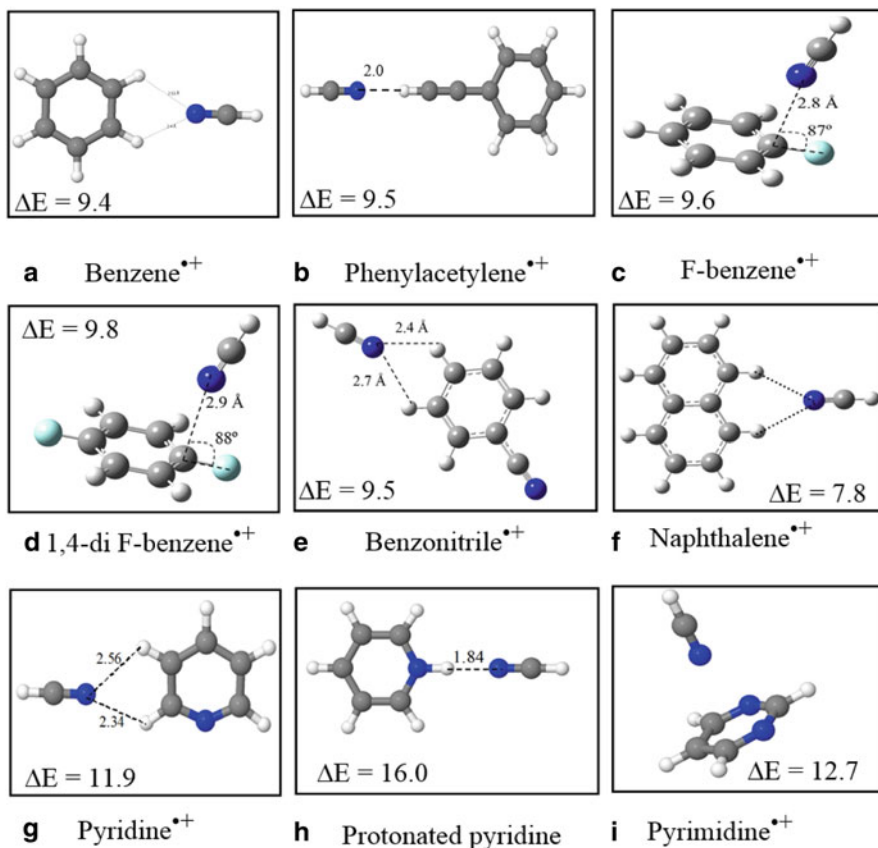
Fig. 15.7 Lowest energy structures of the organic cation −(HCN) clusters. ΔE is the calculated binding energy in kcal/mol. The calculated structures were obtained at the B3LYP/6-311++G(d, p) level for the benzene$^{\bullet+}$, phenylacetylene$^{\bullet+}$, F-benzene$^{\bullet+}$, 1,4-di F-benzene$^{\bullet+}$, benzonitrile$^{\bullet+}$, and naphthalene$^{\bullet+}$ radical cations [45–47], and at the M06-2X/6-311++G(d, p) level for the pyridine$^{\bullet+}$, pyrimidine$^{\bullet+}$ and protonated pyridine [48]

ions were found to have the conventional radical cation structures similar to the hydrated benzene cation. For the hydrated pyrimidine radical cation $(C_4N_2H_4^{\bullet+})(H_2O)_n$, the lowest energy isomer has a bifurcated structure with H_2O bonding to two CH hydrogens with relatively larger distances (2.4 Å and 2.2 Å) than typical H-bonds as shown in Fig. 15.6f. However, the lowest energy isomer of the hydrated protonated pyrimidine has the water molecule directly attached to the NH^+ center via a NH^+–O hydrogen bond of 1.67 Å (Fig. 15.6g), similar to the structure of the hydrated protonated pyridine [21]. This is mediated by the stronger interaction that involves a $NH^+\cdot\cdot OH_2$ bond similar to other ionic hydrogen bonds where the proton is shared between two centers containing lone pairs of electrons.

The calculated lowest energy structures of HCN complexes with several organic ions are shown in Fig. 15.7. The complexes of HCN with ionized aromatics are

bonded primarily by electrostatic forces both in planar hydrogen-bonded structures and in vertical L-shaped structures as shown in Fig. 15.7. The lowest energy isomers of the HCN complexes with the benzene, benzonitrile, pyridine and naphthalene radical cations calculated at the B3LYP/6-311++G(d, p) level have bifurcated structures with HCN binding to two CH hydrogen atoms as shown in Fig. 15.7. For the $C_8H_6^{\bullet+}$(HCN) complex, the lowest energy isomer shows the N-atom of the HCN molecule interacting with the acetylenic CH by a 2.0 Å hydrogen bond as shown in Fig. 15.7b [46]. This indicates that the attachment of HCN to the acetylene group is more favorable than the interaction with the phenyl ring.

The lowest energy structure of the $C_5H_5NH^+$(HCN) complex shows a conventional IHB between the NH^+ group of the protonated pyridine and the nitrogen atom of HCN as shown in Fig. 15.7h. The lowest energy structure of the $C_4H_4N_2^{\bullet+}$(HCN) complex has a T-shaped ion-dipole structure with the N atom of HCN pointing toward the center of the pyrimidine cation ring [48].

The HCN molecule binds to the fluorobenzene radical cation at an angle of 87° to the plane of the fluorobenzene$^{\bullet+}$ ion with a bond length of 2.8 Å as shown in Fig. 15.7c. A similar geometry is found with the difluorobenzene radical cation, with the ion plane-to-molecule angle and bond length of 88° and 2.9 Å, respectively as shown in Fig. 15.7 d [47]. The atomic charges on the ions are also of interest. In fluorobenzene$^{\bullet+}$, the electronegative F atom is significantly negative and its carbon has a high partial positive charge (0.60) in the ion [47]. The negative N end of the HCN neutral molecule (− 0.31) can interact attractively with the large positive charge at this carbon. On the other hand, in hydrogen bonding to the ring hydrogens, especially the para hydrogen, HCN interacts with a smaller positive charge (0.24), but this interaction is not destabilized by nearby negative charges. These effects balance out fortuitously to lead to practically equal binding energies in the planar and vertical isomers [47]. Similar charges, interactions and binding energies apply in 1,4-difluorobenzene$^{\bullet+}$. However, in benzonitrile$^{\bullet+}$, although the CN group is electron withdrawing, there are no large positive charges on the ring carbons, and a planar bifurcated hydrogen-bonded structure has the lowest energy similar to the benzene$^{\bullet+}$(HCN) complex [47].

15.2.3 "Internally" & "Externally" Solvated Ions

It is of interest to compare "*internally solvated*" structures where the solvent molecules are bonded directly to the ion with "*externally solvated*" structures where the solvent molecules are bonded to each other and the ion is hydrogen bonded to the exterior of a solvent cluster. Figure 15.8 displays the lowest energy structures of the hydrated organic ions by two water molecules. It is interesting to note that all the structures shown in Fig. 15.8, with the exception of the c-$C_3H_3^+$ and pyrimidine ions, form "externally hydrated" structures where the two water molecules are bonded to each other. This indicates that the formation of "*internally hydrated*" structures in
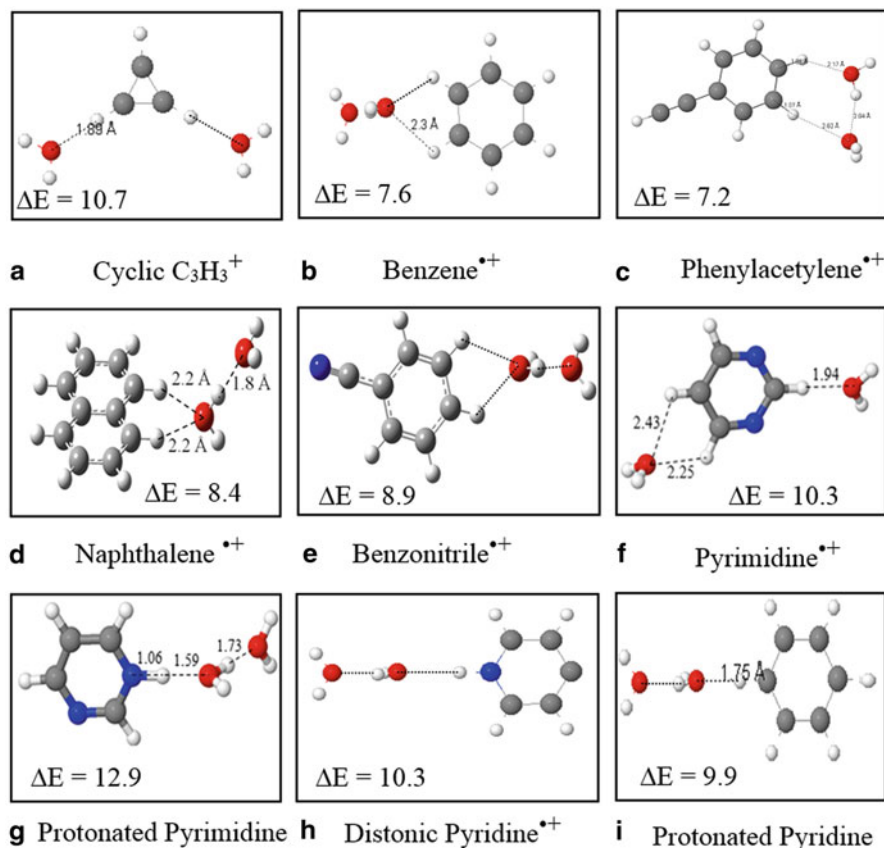
$\Delta E = 10.7$	$\Delta E = 7.6$	$\Delta E = 7.2$
a Cyclic $C_3H_3^+$	**b** Benzene$^{\bullet+}$	**c** Phenylacetylene$^{\bullet+}$

$\Delta E = 8.4$	$\Delta E = 8.9$	$\Delta E = 10.3$
d Naphthalene$^{\bullet+}$	**e** Benzonitrile$^{\bullet+}$	**f** Pyrimidine$^{\bullet+}$

$\Delta E = 12.9$	$\Delta E = 10.3$	$\Delta E = 9.9$
g Protonated Pyrimidine	**h** Distonic Pyridine$^{\bullet+}$	**i** Protonated Pyridine

Fig. 15.8 Lowest energy structures of the organic cation-$(H_2O)_2$ clusters. ΔE is the calculated binding energy in kcal/mol. The calculated structures were obtained at the MP2//ROHF/6-31+G(d, p) level for the c-$C_3H_3^+$, benzene$^{\bullet+}$, phenylacetylene$^{\bullet+}$, pyridine$^{\bullet+}$, distonic pyridine$^{\bullet+}$ and protonated pyrimidine, [15–17,20] at the B3LYP/6-311++G(d, p) level for the naphthalene$^{\bullet+}$ and benzonitrile$^{\bullet+}$ radical cations, [19] and at the M06-2X/6-311++G(d, p) level for the pyrimidine$^{\bullet+}$ and protonated pyrimidine [21]

which the water molecules are bonded to the organic ion may require more than two water molecules.

Clustering of the second water molecule on the $C_3H_3^+$ (H_2O) ion gives a symmetric *internally* hydrated structure as shown in Fig. 15.8a [16]. A similar structure is found for the addition of the second water molecule to the pyrimidine $(C_4N_2H_4^{\bullet+})$ ion as shown in Fig. 15.8f [21]. However, the calculated structures of the hydrated protonated pyrimidine $(C_4N_2H_5^+)(H_2O)_n$ clusters are significantly different from those of the hydrated radical cation [21]. The lowest energy pyrimidineH$^+$$(H_2O)$ cluster, has the water molecule directly attached to the NH$^+$ center via a NH$^+$–O hydrogen bond of 1.67 Å (Fig. 15.6g) similar to the structure of the hydrated protonated pyridine
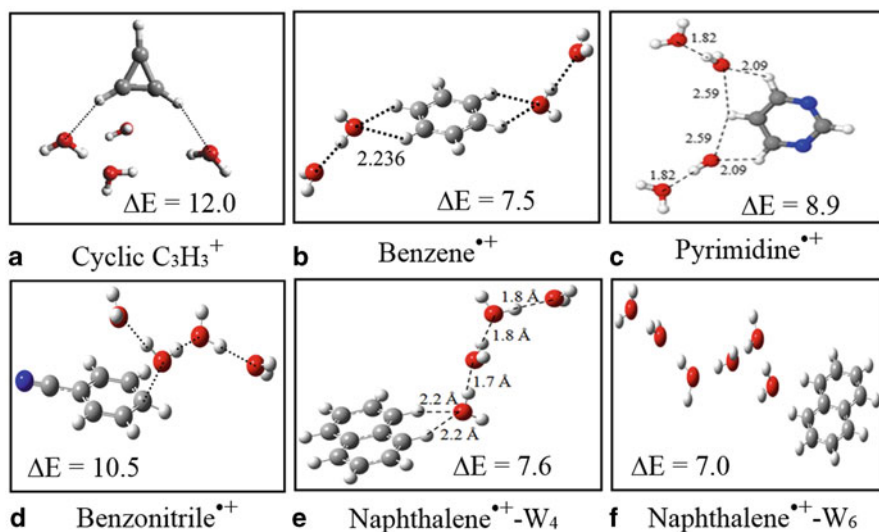
Fig. 15.9 Lowest energy structures of the organic cation-$(H_2O)_4$ clusters. ΔE is the calculated binding energy in kcal/mol. The calculated structures were obtained at the MP2//ROHF/6-31+G(d, p) level for the c-$C_3H_3^+$ and benzene$^{\bullet+}$, [15–17,20] at the B3LYP/6-311++G(d, p) level for the benzonitrile$^{\bullet+}$ and naphthalene$^{\bullet+}$, [19] and at the M06-2X/6-311++G(d, p) level for the pyrimidine$^{\bullet+}$ [21]. The structure of the Naphthalene$^{\bullet+}$-$(H_2O)_6$ (Naphtalene$^{\bullet+}$-W_6) is also shown

shown in Fig. 15.6i [21]. For the protonated pyrimidine, the second water molecule binds to the first water molecule by a 1.73 Å hydrogen bond while the NH$^+$–O bond shortens to 1.59 Å as shown in Fig. 15.8g.

Figure 15.9 displays the lowest energy structures of the hydrated organic ions by four water molecules. The sequential addition of four water molecules to the $C_3H_3^+$ ion results in a cyclic water tetramer bound with two long hydrogen bonds to the $C_3H_3^+$ hydrogens [16]. It is interesting that the lowest energy isomer of the $C_3H_3^+(H_2O)_3$ cluster involves the formation of a cyclic water trimer [16]. This propensity of water molecules to form cyclic structures in the presence of the c-$C_3H_3^+$ ion is consistent with the structural behavior of neutral water clusters [49, 59].

The lowest energy structure of $C_6H_6^{\bullet+}(H_2O)_4$ is symmetrical with a water dimer on each side of the ion, both forming bifurcated bonds with the ion [15]. IR spectroscopy and *ab initio* calculations indicate that the first water molecule forms two IHBs with two adjacent hydrogen atoms of the benzene cation as shown in Figs 15.6b [55, 60]. For the $C_6H_6^{\bullet+}(H_2O)_n$ with $n = 2$–4 both "*internally solvated*" isomers where the water molecules are bonded directly to the benzene cation and "*externally solvated*" isomers where the benzene cation is attached to a cluster of water molecules have been predicted [54, 55, 60].

The lowest energy isomers of the pyrimidine$^{\bullet+}(H_2O)_4$ cluster show both "*internally solvated*" and "*externally solvated*" structures with similar binding energies [21]. However, the calculated structures of the hydrated protonated pyrimidine $(C_4N_2H_5^+)(H_2O)_n$ clusters are different from those of the hydrated radical cation

[21]. The pyrimidineH$^+$(H$_2$O)$_3$ shows a symmetric structure where a central water molecule binds by 1.75 Å hydrogen bonds to two other water molecules; and to protonated pyrimidine by a shorter NH$^+$–O bond of 1.43 Å [21]. This structure is consistent with a growth pattern that could lead to dissociative proton transfer within the pyrimidineH$^+$(H$_2$O)$_4$ cluster to form the closed shell solvated hydronium ion H$_3$O$^+$(H$_2$O)$_3$ as observed experimentally [21].

Unlike the hydration of the benzene radical cation where the C$_6$H$_6^{+\bullet}$(H$_2$O)$_n$ clusters with n up to 4 exhibit mainly "*internally*" solvated structures with the water molecules forming bifurcated hydrogen bonds with the CH$^{\delta+}$ groups of the benzene cation, [15] the sequential addition of water molecules onto the naphthalene cation favors *external* solvation where the naphthalene cation remains exterior with respect to the water sub-cluster [19]. The calculated structures of the naphthalene$^{\bullet+}$(H$_2$O)$_4$ and naphthalene$^{\bullet+}$(H$_2$O)$_6$ are shown in Figs. 15.9e and 15.9f, respectively. Similar structures are also obtained for naphthalene$^{\bullet+}$(CH$_3$OH)$_4$ and naphthalene$^{\bullet+}$(CH$_3$OH)$_6$ [19].

This indicates that hydrogen bonding interactions among water molecules are more favorable than the unconventional hydrogen bonding formed between the CH$^{\delta+}$ sites of the naphthalene cation and the water molecules. This observation suggests that the solvation of larger PAH cations would also favor the "*externally*" solvated structures where the large organic species remain accessible at the surface of the water nanodroplets. This could have an important implication to the reactivity of large PAH ions in interstellar medium since the ions can interact with incoming small molecules under UV irradiation where both ion-molecule and photochemical processes can lead to the formation of complex organics on the surface of the ice grains [10, 19].

The above results and discussions indicate that unlike the hydration of metal ions, where the ion-water interaction is significantly stronger than the water-water interaction, water-water interaction can be very similar or even stronger than ion-water interaction in the hydration of organic ions [1]. Therefore, it appears that the common ion hydration picture where the ion is surrounded by 4–6 water molecules may not be valid for the hydration of organic ions. The observed trend of a large entropy loss with the higher order hydration steps as a result of forming cyclic or bicyclic hydrogen bonded water clusters supports this view [15, 17]. In other words, unless the organic ion is very small (e.g. C$_3$H$_3^+$), "internally hydrated" structures may not form and the large organic ions remain outside the cage-like hydrogen bonded water structures [19].

15.2.3.1   Solvation of Organic Ions by HCN Molecules

Solvation of the organic ions by HCN molecules show a tendency to form extended HCN chains associated with the benzene and phenylacetylene radical cations and protonated pyridine. Figure 15.10 displays the calculated lowest energy structures of the benzene$^{\bullet+}$(HCN)$_n$, phenylacetylene$^{\bullet+}$(HCN)$_n$ and protonated pyridineH$^+$(HCN)$_n$ clusters with $n = 2$ and 4. It is clear that the addition of the second HCN molecule
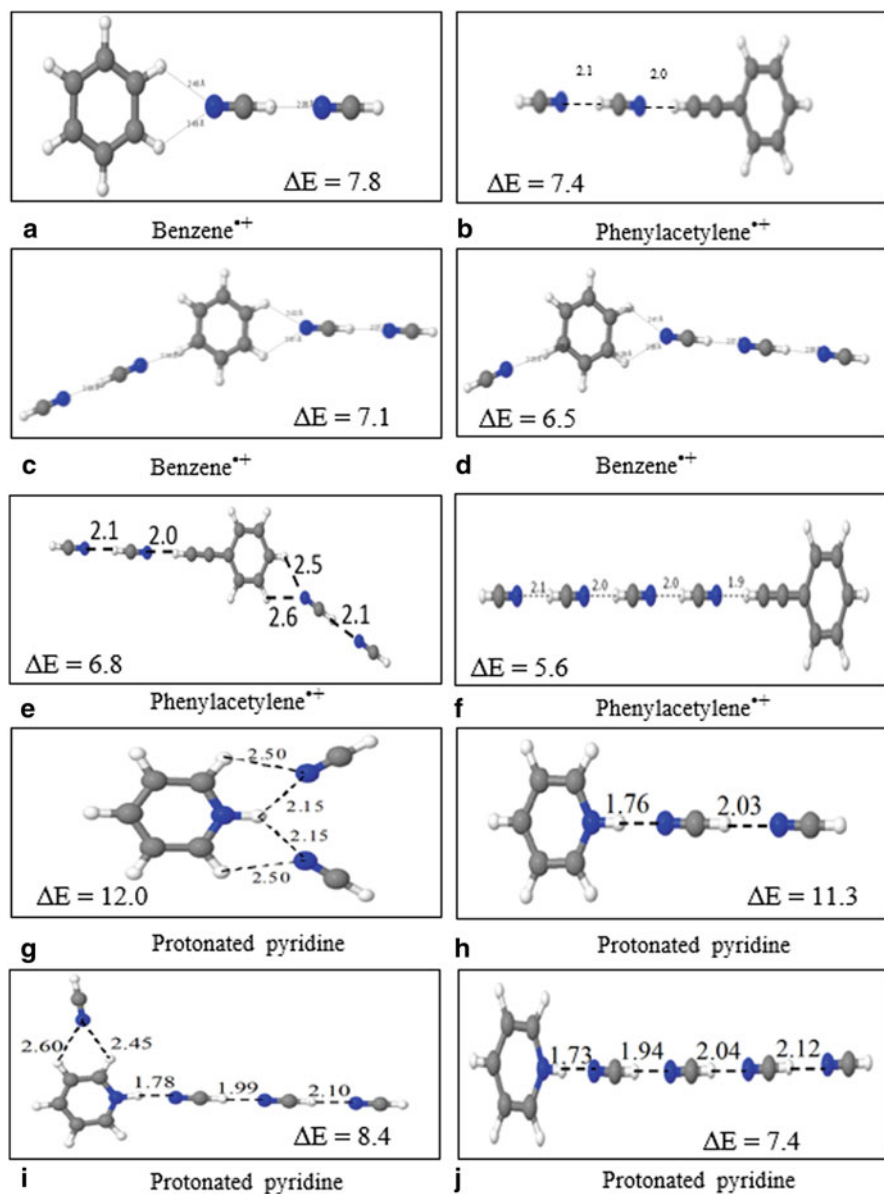
Fig. 15.10 Lowest energy structures of organic cation-(HCN)$_n$ clusters with $n = 2$ and 4. ΔE is the calculated binding energy in kcal/mol. The calculated structures were obtained at the B3LYP/6-311++G(d, p) level for the benzene$^{\bullet+}$ and phenylacetylene$^{\bullet+}$ radical cations, [45, 46] and at the M06-2X/6-311++G(d, p) level for protonated pyridine [48]

is more likely to form HCN...HCN hydrogen bond than forming a second C-H$^\delta$....NCH bond with the organic ion. The structures of the ions solvated by four

HCN molecules represent a competition between the assembly of a linear hydrogen bonding HCN chain and internal solvation of the cation. Interestingly, structures with linear hydrogen bonded chains extended from the phenylacetylene cation are only 1 kcal/mol higher in energy than the lowest energy isomer. For protonated pyridine, the extended chain structure with four HCN molecules (Fig. 15.10j) is 1.0 kcal/mol higher in energy than the lowest energy isomer with an extended chain of three HCN molecules shown in Fig. 15.10i. These extended structures are good models for the design of molecular wires formed by hydrogen bonding chains that could be utilized for low temperature molecular devices [61–63]. For example, the lengths of these molecular wires (the distance from the carbon atom of the phenyl ring connected to the C≡C group to the hydrogen atom of the terminal HCN molecule in the one-sided chain structures) can vary from 0.8 to 2.1 nm depending on the number of HCN molecules. For the two sided chain structures where the phenyl ring can be considered as part of the wire, the distance between the hydrogen atoms of the terminal HCN molecules on both sides of the ring can reach 2.5 nm in the $C_8H_6^{\bullet+}(HCN)_4$ cluster. These wire assemblies connected by hydrogen bonds could provide unique opportunities for systematic spectroscopic and structure studies of charge distributions and separations in these systems.

It should be noted that extended linear chain structures involving HCN and acetylene units are common in the solid state molecular crystals of these molecules. For example, in the solid state, both hydrogen cyanide and cyanoacetylene (H-C≡C-C≡N) crystals consist of extended, linear hydrogen-bonded chains [64, 65]. However, in the gas phase both linear and cyclic structures are known to exist based on several spectroscopic and theoretical studies [66–69]. Interestingly, clusters of linear chains have been reported to exist in superfluid helium expansion [70]. In cluster ions, the measured thermochemistry of protonated HCN clusters $[H^+(HCN)_n]$ suggests the formation of linear hydrogen-bonded chains extended from a strongly bound core consisting of the proton-bound HCN dimer (HCN.H^+.NCH) [71, 72]. In the present system, the core ion is the phenylacetylene cation which allows the formation of HCN extended chains by hydrogen bonding to the acetylene hydrogen or to the hydrogen atoms of the phenyl ring. It appears that the formation of a one-sided chain by hydrogen bonding of the HCN molecules to the acetylene hydrogen, and two-sided chains by additional hydrogen bonding to the para hydrogen atom (with respect to the acetylene group) of the phenyl ring represents the most favorable modes for the growth of the hydrogen cyanide molecular wires attached to the phenylacetylene cation.

The second group of organic ions which includes pyridine$^{\bullet+}$, pyrimidine$^{\bullet+}$, F-benzene$^{\bullet+}$, 1,4-di-F-benzene$^{\bullet+}$, benzonitrile$^{\bullet+}$, and naphthalene$^{\bullet+}$ show more tendency for internal solvation by four HCN molecules than for the formation of extended HCN chains. The calculated lowest energy structures of these solvated ions are shown in Fig. 15.11.

The lowest energy structures of the $C_5H_5N^{\bullet+}(HCN)_4$ and $C_4H_4N_2^{\bullet+}(HCN)_4$ clusters show bifurcated structures involving multiple hydrogen bonding sites with the ring hydrogen atoms as shown in Figs. 15.11a and 15.11b, respectively. However, no chain structures involving four HCN molecules have been found in these clusters
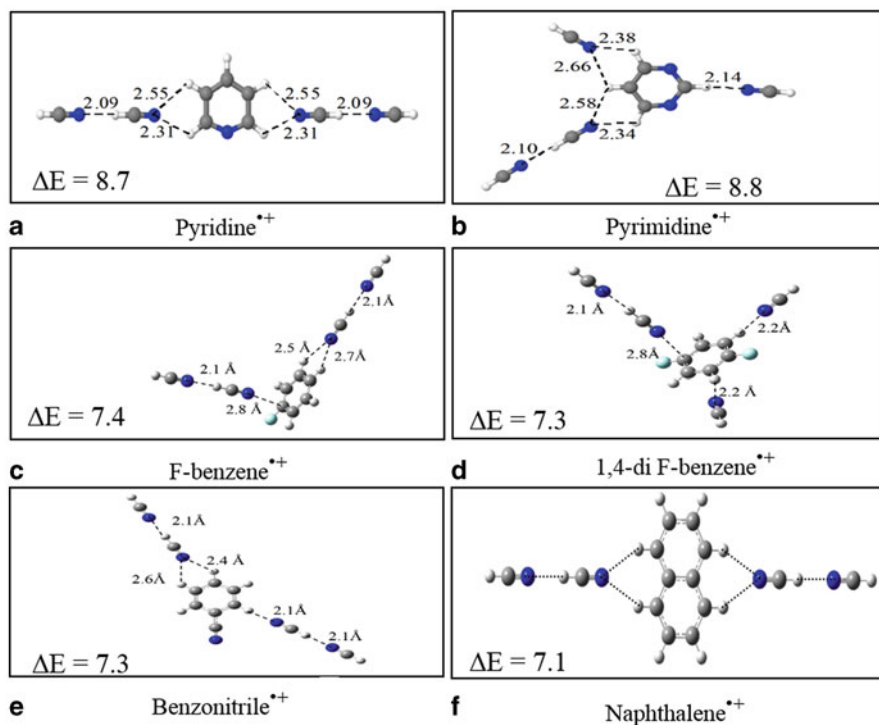
Fig. 15.11 Lowest energy structures of organic radical cation-(HCN)$_4$ clusters. ΔE is the calculated binding energy in kcal/mol. The calculated structures were obtained at the B3LYP/6-311++G(d, p) level for the F-benzene$^{\bullet+}$, 1,4-di F-benzene$^{\bullet+}$ and benzonitrile$^{\bullet+}$, [47] and at the M06-2X/6-311++G(d, p) level for pyridine$^{\bullet+}$ and pyrimidine$^{\bullet+}$ radical cations [48]

indicating that HCN interactions with the pyridine or pyrimidine ring cations are more favorable than the interactions within the HCN chains.

In the $C_6H_5F^{\bullet+}(HCN)_4$ cluster, the fourth HCN binds externally to the third bifurcated HCN with a bond length of 2.1 Å as shown in Fig. 15.11c. The measured binding energy for this addition is 7.8 kcal/mol in good agreement with the DFT calculated value of 7.4 kcal/mol. The fourth HCN in $C_6H_4F_2^{\bullet+}(HCN)_4$ binds externally to the second meta position on the aromatic ring as shown in Fig. 15.11d, with a bond length of 2.2 Å. The measured binding energy of 7.7 kcal/mol agrees well with the theoretical value of 7.3 kcal/mol. In the benzonitrile cluster ion $C_6H_5CN^{\bullet+}(HCN)_4$, the fourth HCN ligand binds externally to the HCN at the ortho position, with a bond length of 2.1 Å (Fig. 15.11e). The measured binding energy for this addition is 6.1 kcal/mol, which is lower than the DFT binding energy of the lowest energy isomer (Fig. 15.11e) of 7.3 kcal/mol, but within the experimental uncertainty range of ± 1 kcal/mol for clustering equilibrium temperature studies.
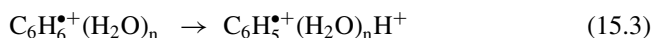
The lowest energy structure of the naphthalene$^{\bullet+}(HCN)_4$ is very similar to that of the benzene$^{\bullet+}(HCN)_4$ cluster where two HCN molecules are attached to the cation

ring from two opposite sides. This structure provides efficient solvation of the organic ion. It is interesting to note that the naphthalene cation is *externally* solvated by four water molecules (Fig. 15.9e) but it can be *internally* solvated by four HCN molecules (Fig. 15.11f). As in all such clusters, the binding energies, with the addition of 4–6 ligands, converge to the enthalpy of vaporization of the ligand (ΔH^{o}_{vap}), which is 6.0 kcal/mol for HCN at 298 K [1, 22, 48].

15.2.4 Intracluster Proton Transfer and Deprotonation Reactions

Intracluster proton transfer (IPT) coupled with cluster's dissociation reactions have been observed in several solvated organic radical cations R-H$^{\bullet+}$(S)$_n$ with specific numbers of solvent molecules (S$_n$). These reactions, also known as Dissociative Proton Transfer (DPT) reactions, generate a protonated solvent cluster S$_n$H$^+$ and an organic radical (R$^{\bullet}$). Intracluster DPT reactions can occur within the R-H$^{\bullet+}$(S)$_n$ clusters if the proton transfer from the radical cation to the solvent sub-cluster (S)$_n$ becomes exothermic and the resulting energy is sufficient to dissociate the R$^{\bullet}\cdots$H$^+$(S)$_n$ cluster. The cluster size (n) at which the PT occurs can be predicted by comparing the proton affinities of the organic radical (R$^{\bullet}$) and the solvent sub-cluster (S)$_n$. These reactions have been observed in C$_6$H$_6^{\bullet+}$(H$_2$O)$_n$, C$_3$H$_3^+$(H$_2$O)$_n$, C$_4$N$_2$H$_4^{\bullet+}$(H$_2$O)$_n$, and C$_4$N$_2$H$_5^+$(H$_2$O)$_n$ with n $\geq$ 4 in all cases [15, 16, 20, 21]. The IPT and DPT reactions are represented by Eqs. (15.3) and (15.4) for the benzene$^{\bullet+}$(H$_2$O)$_n$ clusters.

Intracluster Proton Transfer (IPT)

$$C_6H_6^{\bullet+}(H_2O)_n \rightarrow C_6H_5^{\bullet+}(H_2O)_nH^+ \qquad (15.3)$$

Intracluster Dissociative Proton Transfer (IDPT)

$$C_6H_6^{\bullet+}(H_2O)_n \rightarrow (H_2O)_nH^+ + C_6H_5^{\bullet} \qquad (15.4)$$
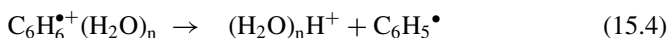
The driving force for the deprotonation of the organic ion is the formation of strong ionic hydrogen bonds in the solvent clusters. The solvent clusters, e.g. (H$_2$O)$_n$H$^+$ can be attached to a radical carbon site through a relatively weak (H$_2$O)$_n$H$^+\cdots$C hydrogen bond, or it can form a stronger (H$_2$O)$_n$H$^+\cdots$N bond to a basic site of the radical such as in pyridine or pyrimidine. These are a new class of solvated clusters where a protonated water cluster is hydrogen bonded to an organic radical. In other words, in these clusters the deprotonated radicals are solvated externally, i.e., the radicals remain outside, and bonded to the surface, of the solvent clusters.

The thermochemistry of the overall reaction (15.3 or 15.4) is relevant if the reaction proceeds effectively in one step, i.e., if the cluster is assembled without stabilization, retaining the exothermicity of all the association steps as internal energy for deprotonation/dissociation to form products. This may be possible in the experiments that use neat water (solvent) vapor, where collision with every successive H$_2$O molecule can lead to association with the release of the binding energy into internal energy, rather

than removing energy from the cluster. However, if a third body is present, it would stabilize the growing cluster and no internal energy would be available for deprotonation/dissociation. In fact, the third-body effect was observed in the benzene$^+$/water system where the addition of He buffer gas quenched the deprotonation reaction [15].

The observation of IPT reactions in the benzene$^{\bullet+}$/water system is consistent with the IR dissociation spectra of the $C_6H_6^{\bullet+}(H_2O)_n$ clusters which were very similar to the spectra of $(H_2O)_nH^+$ after $n = 4$, indicating that intracluster proton transfer resulted in the formation of a protonated water cluster attached to the phenyl radical [54]. However, H/D-exchange experiments under thermal ion mobility conditions showed that $C_6H_6^{\bullet+}(D_2O)_n$ clusters with $n = 2$–8 did not exchange a proton with D_2O to yield a $C_6H_5^{\bullet}(D_2O)_nD^+$ ion, although this would be expected for the $C_6H_5^{\bullet}(D_2O)_nH^+$ structure [15]. It was, therefore, suggested that the intracluster proton transfer has an energy barrier that cannot be overcome in thermal systems below 280 K in the ion mobility experiments [15].

The deprotonation of organic ions such as $C_3H_3^+$ and $C_6H_6^{\bullet+}$ requires the assembly of several solvent molecules (at least 4 for H_2O) which is strongly facilitated at lower temperatures. Therefore, the rate coefficients of these reactions showed uniquely large negative temperature coefficients, with pseudo second-order coefficients varying as $k = cT^{-63}$ and $k = cT^{-67}$- in the hydrated $C_3H_3^+$ and $C_6H_6^{\bullet+}$ ions, respectively [15, 16]. The large negative temperature coefficients result from a multibody mechanism in which five or more components need to be assembled in the activated complex [for example, $C_6H_6^{\bullet+}(H_2O)_4$]* for the reaction to proceed. This means that only the fraction of the total cluster population that is in the $n \geq 4$ clusters is reactive. Therefore, only this fraction among all the collisions of the clusters with H_2O molecules are reactive, and the small collision efficiency of 10^{-5}–10^{-6} reflects this effect [15, 16]. The population of the large reactive clusters increases rapidly with decreasing temperature, and this leads to the large negative temperature coefficient.

IPT reactions were not observed in the naphthalene $^{\bullet+}(H_2O)_n$ clusters because of the higher proton affinity (PA) of the naphthalene radical ($C_{10}H_7^{\bullet}$, 234 kcal/mol) [73] as compared to that of the phenyl radical ($C_6H_5^{\bullet}$, 212 kcal/mol) [15]. This means that more than seven or eight water molecules will be required to associate with the naphthalene radical cation for the IPT to occur. However, IPT reactions can occur within the $C_{10}H_8^{\bullet+}(CH_3OH)_n$ clusters if the proton transfer from the $C_{10}H_8^{\bullet+}$ radical cation to the methanol sub-cluster $(CH_3OH)_n$ becomes exothermic and the resulting energy is sufficient to dissociate the $C_{10}H_7^{\bullet} \cdots H^+(CH_3OH)_n$ cluster. Based on the estimates of the PAs of the naphthalene radical ($C_{10}H_7^{\bullet}$) [73] and the methanol clusters [74], the PT reaction from $C_{10}H_8^{\bullet+}$ to the methanol sub-cluster in $C_{10}H_8^{\bullet+}(CH_3OH)_n$ is expected to becomes exothermic at $n > 5$. This is consistent with the changes in the mass spectra of the $C_{10}H_8^{\bullet+}(CH_3OH)_n$ clusters at 238 K where the ion signal of the naphthalene-containing ions disappeared and only the $H^+(CH_3OH)_n$ clusters with $n \geq 5$ were observed [19].

The calculated the structures of the clusters formed by the association of the naphthalene radical ($C_{10}H_7^{\bullet}$) with protonated methanol [$H^+(CH_3OH)_n$] clusters with $n = 4$−6 and their binding energies are shown in Fig. 15.12.
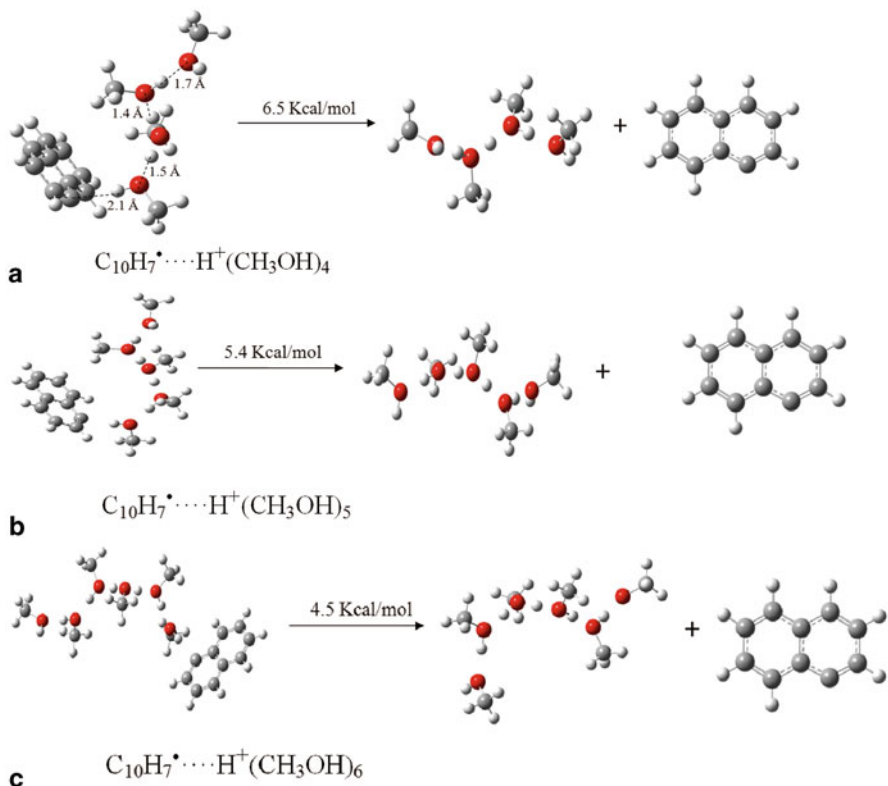
Fig. 15.12 Structures and binding energies of the lowest energy structures of the $C_{10}H_7\cdot$. $H^+(CH_3OH)_n$ clusters with $n = 4 - 6$ obtained at the B3LYP/6-311^{++}G(d, p) level [19]

It is clear that the binding energy of the protonated methanol cluster to the naphthalene radical decreases as the size of the protonated methanol cluster (n) increases. For example, the binding energies of the $H^+(CH_3OH)_n$ clusters to the $C_{10}H_7^\bullet$ radical decrease from 6.5 to 5.4 to 4.5 for $n = 4, 5$ and 6, respectively according to the B3LYP/6-311^{++}G(d, p) calaculations [19]. This can be explained by the decrease in the charge-induced dipole interaction between the protonated methanol cluster and the naphthalene radical as the effective charge becomes more delocalized on the methanol cluster and further away from the radical. Eventually, the effect of the charge would disappear and the binding energy would converge to that of the neutral system. Since both the intracluster PT from the naphthalene radical cation to the methanol sub-cluster in the $C_{10}H_8^{\bullet+}(CH_3OH)_n$ clusters becomes more exothermic as n increases and the binding energies of the resulting $C_{10}H_7^\bullet\cdots H^+(CH_3OH)_n$ clusters decrease as n increases, dissociation of the larger $C_{10}H_8^{+\bullet}(CH_3OH)_n$ clusters into the $C_{10}H_7^\bullet$ radical and protonated methanol clusters is expected to be the predominant process at low temperatures. This is consistent with the experimental observation mentioned above [19].

In general, IPT reactions are controlled by the relative PAs of the organic radical and the cluster of solvent molecules and the extent of bonding interaction between the organic radical and the protonated solvent cluster. The transfer of the proton from the organic radical cation to the solvent molecules generates a protonated solvent cluster such as $(H_2O)_nH^+$ which can be hydrogen bonded to the radical ring carbon site $[(H_2O)_nH^+\cdots C]$ or at a basic nitrogen site $[(H_2O)_nH^+\cdots N]$. These are a new class of solvated clusters where a protonated solvent cluster is hydrogen bonded to an organic radical. In other words, in these clusters the deprotonated radicals are solvated externally, i.e., the radicals remain outside, and bonded to the surface, of the solvent clusters. Alternatively, the protonated solvent cluster can be detached from the deprotonated radical to generate a free protonated cluster $(H_2O)_nH^+$ and a free organic radical $(R^\bullet)$. The variation of the radical/cluster bonding energy with cluster size is of interest, and more experimental and theoretical works are needed in order to understand the energetics and dynamics of these solvated clusters.

References

1. Meot-Ner (Mautner), M (2012) Update 1 of: strong ionic hydrogen bonds. Chem Rev 112:PR22–103; (2005) The Ionic hydrogen bond. Chem Rev 105:213–284
2. Tsuzuki S (2005) In: Wales DJ (ed) Intermolecular Forces and Clusters I, vol. 115. Springer, Berlin, p 149
3. Cerny J, Hobza P (2007) Non-covalent interactions in biomacromolecules. Phys Chem Chem Phys 9:5291
4. Conway BE (1981) Ionic hydration in chemistry and biophysics. Elsevier, Amsterdam
5. Sloan EDMD (2008) Clathrate hydrates of natural gases, vol 3. CRC Press, Florida
6. Nuevo M, Milam SN, Sandford SA, Elsila J, Dworkin JP (2009) Formation of uracil from the ultraviolet photo-irradiation of pyrimidine in pure H_2O ices. Astrobiol 9:683–695
7. Menor-Salvan C, Marin-Yaseli MR (2012) Prebiotic chemistry in eutectic solutions at the water–ice matrix. Chem Soc Rev 41:5404–5415
8. Ben-Naim A (1980) Hydrophobic interactions. Plenum, New York
9. Tanford C (1980) The hydrophobic effect: formation of micelles and biological membranes, 2nd edn. Wiley, New York
10. Gudipati RS, Allamandola LJ (2006) Unusual stability of polycyclic aromatic hydrocarbon radical cations in amorphous water ices up to 120 K: astronomical implications. Astrophys J 638:286–292
11. Rhee YM, Lee TJ, Gudipati MS, Allamandola LJ, Head-Gordon, M (2007) Charged polycyclic aromatic hydrocarbon clusters and the galactic extended red emission. Proc Natl Acad Sci U S A 104:5274–5278
12. Snow TP, Bierbaum VM (2008) Ion chemistry in the interstellar medium. Annul Rev Anal Chem 1:229
13. Herbst E, van Dishoeck EF (2009) Complex organic interstellar molecules. Annul Rev Astron Astrophys 47:427–480
14. Ibrahim, Y, Alsharaeh E, Dias K, Meot-Ner M, El-Shall MS (2004) Stepwise hydration, and multi-body deprotonation with steep negative temperature dependence in the Benzene∞^+– water system. J Am Chem Soc 127:12766–12767

15. Ibrahim Y; Alsharaeh E, Meot-Ner M, El-Shall MS, Scheiner S (2005) Stepwise hydration of ionized aromatics, energies, structures of the hydrated benzene cation, and the mechanism of deprotonaion reactions. J Am Chem Soc 127:7053–7064

16. Mabrouki R, Ibrahim Y, Xie E, Meot-Ner M, El-Shall MS (2006) Gas phase hydration and deprotonation of the cyclic $C_3H_3^+$ cation. Solvation with acetonitrile and comparison with the benzene radical cation. J Phys Chem A 110:7334–7344

17. Momoh PO, El-Shall MS (2008) Gas phase hydration of organic ions. Phys Chem Chem Phys 10:4827–4834

18. Momoh PO, Hamid AM, Abrash SA, El-Shall MS (2011) Structure and hydration of the $C_4H_4^{\bullet+}$ Ion formed by electron impact ionization of acetylene clusters. J Chem Phys 134:204315

19. Attah IK, Platt SP, Meot-Ner (Mautner) M, Aziz SG, Alyoubi AO, El-Shall MS (2014) Hydrogen bonding of the naphthalene radical cation to water and methanol and attachment of the naphthalene ion to extended hydrogen bonding chains. Chem Phys Lett 613:45–53

20. Ibrahim Y, Mabrouki R, Meot-Ner M, El-Shall MS (2007) Hydrogen bonding interactions of pyridine$^{\bullet+}$ with water: stepwise solvation of distonic cations. J Phys Chem A 111:1006–1014

21. Hamid AM, Sharma P, Hilal R, Elroby S, Aziz SG, Alyoubi AO, El-Shall MS (2013) Hydration of the pyrimidine radical cation and stepwise solvation of protonated pyrimidine with water, methanol and acetonitrile. J Chem Phys 139:084304

22. NIST Chemistry Web Book NIST Standard Reference Database Number 69; National Institute of Standards and Technology: Gaithersburg MD, 20899 (http://webbook.nist.gov)

23. Li QB, Jacob DJ, Yantosca RM, Heald CL, Singh HB, Koike M, Zho YJ, Sachse GW, Streets DG (2003) A global 3-D model evaluation of the atmospheric budgets of HCN and CH_3CN: constraints from aircraft measurements over the western pacific. J Geophys Atmos 108:8827

24. Matthews CN, Ludicky RA (1992) Hydrogen cyanide polymers on comets. Adv Space Res 12:21–32

25. Matthews CN, Minard RD (2006) Hydrogen cyanide polymers, comets and the origin of life. Faraday Discuss 133:393–401

26. Pizzarello S, Holmes W (2009) Nitrogen-containing compounds in two CR2 meteorites: 15N composition, molecular distribution and precursor molecules. Geochim Cosmochim Acta 73:2150–2162

27. Mumma MJ, DiSanti MA, Magee-Sauer K, Bonev BP, Villanueva GL, Kawakita H, Russo ND, Gibb EL, Blake GA, Lyke JE, Campbell RD, Aycock J, Conrad A, Hill GM (2005) Parent volatiles in comet 9P/Tempel 1: before and after impact. Science 310:270

28. Lahuis F, van Dishoeck EF, Boogert ACA, Pontopiddan KM, Blake GA, Dullemond CP, Evans II NJ, Hogerheijde MR, Jørgensen JK, Kessler-Silacci JE, Knez C (2006) Hot organic molecules toward a young low-mass star: a look at inner disk chemistry. Astrophys J Lett 636:L145

29. Haupert LJ, Enthold PG (2013) Hydration energies of aromatic ions in the gas phase. J Phys Chem A 117:1164–1170

30. Wyttenbach T, Bowers MT (2009) Hydration of biomolecules. Chem Phys Lett 480:1–16

31. Gao B, Wyttenbach T, Bowers MT (2009) Hydration of protonated aromatic amino acids: phenylalanine, tryptophan, and tyrosine. J Am Chem Soc 131:4695–4701

32. Liu D, Wyttenbach T, Bowers MT (2006) Hydration of mononucleotides. J Am Chem Soc 128:15155–15163

33. Kebarle P (1997) Ion thermochemistry and solvation from gas phase ion equilibria. Annu Rev Phys Chem 28:445

34. Keesee RG, Castleman AW (1986) Thermochemical data on gasâŁłphase ionâŁłmolecule association and clustering reactions. J Phys Chem Ref Data 15:1011

35. Larson JW, McMahon TB (1987) Hydrogen bonding in gas-phase anions. The energetics of interaction between cyanide ion and Broensted acids determined from ion cyclotron resonance cyanide exchange equilibria. J Am Chem Soc 109:6230

36. Gorman GS, Amster JI (1993) Gas-phase basicity measurements of dipeptides that contain valine. J Am Chem Soc 115:5729

37. Gross DS, Schnier PD, Rodriguez-Cruz SE, Fagerquist CK, Williams ER (1996) Conformations and folding of lysozyme ions in vacuo. Proc Natl Acad Sci U S A 93:3143

38. Deakyne CA (1997) In: Scheiner S (ed) Molecular interactions: from van der Waals to strongly bound complexes. Wiley, New York, p 217
39. Meot-Ner (Mautner) M (2003) The proton affinity scale, and effects of ion structure and solvation. Int J Mass Spectrom 227:525
40. Meot-Ner (Mautner) M, Lias SG (2003) Binding energies between ions and molecules, and the thermochemistry of cluster ions. In: Linstrom PJ, Mallard WG (eds) NIST chemistry webbook. NIST Standard Reference Database Number 69; National Institute of Standards and Technology: Gaithersburg, MD, March 2003 (http://webbook.nist.gov)
41. Wyttenbach T, Bowers MT (2007) Intermolecular interactions in biomolecular systems examined by mass spectrometry. Annu Rev Phys Chem 58:511
42. Kemper PR, Dupuis NF, Bowers MT (2009) A new, higher resolution, ion mobility mass spectrometer. Int J Mass Spectrom 287:46
43. Momoh PO, El-Shall MS (2007) Stepwise hydration of ionized acetylene trimer. Further evidence for the formation of benzene radical cation. Chem Phys Letters 436:25–29
44. Momoh PO, Xie E, Abrash SA Meot-Ner M, El-Shall MS (2008) Gas phase reactions between acetylene radical cation and water. Energies, structures and formation mechanism of $C_2H_3O^+$ and $C_2H_4O^+$ ions. J Phys Chem A 112:6066–6073
45. Hamid AM, Soliman AR, El-Shall MS (2013) Stepwise association of hydrogen cyanide and acetonitrile with the benzene radical cation: structures and binding energies of $(C_6H_6^{\bullet+})(HCN)_n$, $n = 1$–6, and $(C_6H_6^{\bullet+})(CH_3CN)_n$, $n = 1$–4, clusters. J Phys Chem A 117:1069–1078
46. Hamid AM, Soliman AR, El-Shall MS (2012) Assembly of HCN hydrogen bonding chains in the gas phase. binding energies and structures of phenylacetylene$^+(HCN)_n$ clusters, $n = 1$–4. Chem Phys Lett 543:23–27
47. Attah IK, Hamid AM, Meot-Ner (Mautner) M, Aziz SG, Alyoubi AO, El-Shall MS (2013) Substituent effects on non-covalent bonds: complexes of ionized benzene derivatives with hydrogen cyanide. J Phys Chem A 117:10588–10597
48. Hamid AM, El-Shall MS, Hilal R, Elroby S, Aziz SG (2014) Unconventional hydrogen bonding to organic ions in the gas phase. Stepwise association of hydrogen cyanide with the pyridine and pyrimidine radical cations and protonated pyridine. J Chem Phys 141:054305–054315
49. Ludwig R (2001) Water: from clusters to the bulk. Angew Chem Int Ed Engl 40:1808
50. Gruenloh CJ, Carney JR, Hagemeister FC, Arrington CA, Zwier TS, Fredericks SY, Wood JT III, Jordan KD (1998) Resonant ion-dip infrared spectroscopy of the S_4 and D_{2d} water octamers in benzene-(water)$_8$ and benzene$_2$-(water)$_8$. J Chem Phys 109:6601
51. Lum K, Chandler D, Weeks JD (1999) Hydrophobicity at small and large length scales. J Phys Chem B 103:4570
52. Solca N, Dopfer O (2001) IR spectrum of the benzene–water cation: direct evidence for a hydrogen-bonded charge–dipole complex. Chem Phys Lett 347:59–64
53. Miyazaki M, Fujii A, Ebata T, Mikami N (2001) Infrared spectroscopy of the benzene–H$_2$O cluster cation: experimental study on the drastic structural change upon photoionization. Chem Phys Lett 349:431–436
54. Miyazaki M, Fujii A, Ebata T, Mikami N (2003) Infrared spectroscopy of hydrated benzene cluster cations, $[C_6H_6\text{-}(H_2O)_n]^+$($n = 1$–6): Structural changes upon photoionization and proton transfer reactions. Phys Chem Chem Phys 5:1137–1148
55. Solca N, Dopfer O (2003) Prototype microsolvation of aromatic hydrocarbon cations by polar ligands: ir spectra of benzene$^+$-L$_n$ clusters (L) H$_2$O, CH$_3$OH). J Phys Chem A 107:4046–4055
56. Tachikawa H, Igarashi M, Ishibashi T (2001) Vibrational frequency-shifts of H2O caused by complex formation with a molecular cation: a density functional study. Phys Chem Chem Phys 3:3052–3056
57. Tachikawa H, Igarashi M (1998) Dynamics of the ionization processes of benzene−H2O clusters: a direct ab initio dynamics study. J Phys Chem A 102:8648–8656
58. Miyazaki M, Fujii A, Mikami N (2004) Binding energy of the benzene−water cluster cation: an ar-mediated ir photodissociation study. J Phys Chem A 108:8269–8272
59. Liu K, Cruzan JD, Saykally RJ (1996) Water clusters. Science 271:929–933

60. Fujii A, Patwari GN, Ebata T, Mikami N (2002) Vibrational spectroscopic evidence of unconventional hydrogen bonds. Inter J Mass Spetrom 220:289
61. Mehata MS (2008) Proton translocation and electronic relaxation along a hydrogen-bonded molecular wire in a 6-hydroxyquinoline/acetic acid complex. J Phys Chem B 112:8383
62. Wang C, Batsanov AS, Bryce MR, Martin S, Nichols RJ, Higgins SJ, Garcia-Suarez VM, Lambert CJ (2009) Oligoyne single molecule wires J Am Chem Soc 131:15647
63. Puigmarti-Luis J, Minoia A, Lei S, Geskin V, Li B, Lazzaroni R, De Feyter S, Amabilino DB (2011) Self-assembly of supramolecular wires and cross-junctions and efficient electron tunnelling across them. Chem Sci 2:1945
64. Dulmage WJ, Lipscomb WN (1951) The crystal structures of hydrogen cyanide, HCN. Acta Crystallogr 4:330
65. Shallcross FV, Carpenter GB (1958) The crystal structure of cyanoacetylene. Acta Crystallogr 11:490
66. Jucks KW, Miller REJ (1988) Near infrared spectroscopic observation of the linear and cyclic isomers of the hydrogen cyanide trimer. Chem Phys 88:6059
67. Ruoff RS, Emilsson T, Klots TD, Chuang C, Gutowsky HS (1988) Rotational spectrum and structure of the linear HCN trimer. J Chem Phys 89:138
68. Karpfen A (1996) Linear and cyclic clusters of hydrogen cyanide and cyanoacetylene: a comparative ab initio and density functional study on cooperative hydrogen bonding. J Phys Chem 100:13474
69. Sanchez M, Provasi PF, Aucar GA, Alkorta I, Elguero J (2005) Theoretical study of HCN and HNC neutral and charged clusters. J Phys Chem B 109:18189
70. Nauta K, Miller RE (1999) Nonequilibrium self-assembly of long chains of polar molecules in superfluid helium. Science 283:1895
71. Meot-Ner (Mautner) M (1978) Solvation of the proton by hydrogen cyanide and acetonitrile. Condensation of hydrogen cyanide with ions in the gas phase. J Am Chem Soc 100:4694
72. Meot-Ner (Mautner) M, Speller CV (1989) Multicomponent cluster ions. 2. Comparative stabilities of cationic and anionic hydrogen-bonded networks. Mixed clusters of water and hydrogen cyanide. J Phys Chem 93:3663
73. Feng WY, Lifshitz C (1996) Ion/molecule reactions of naphthalene and 1-chloronaphthalene radical cations. Inter J Mass Spectrom Ion Proc 152:157
74. Knochenmuss R, Cheshnovsky O, Leutwyler S (1988) Proton transfer reactions in neutral gas—phase clusters: 1-Naphthol with H2O, D2O, CH3OH, NH3 and piperidine. Chem Phys Lett 144:317